Petrogenesis of the 1.85 Ga Sonakhan mafic dyke swarm, Bastar Craton, India

Article *in* Lithos · March 2019

DOI: 10.1016/j.lithos.2019.03.015

Lithos 334–335 (2019) 88–101

Contents lists available at ScienceDirect

Lithos

journal homepage: www.elsevier.com/locate/lithos

Petrogenesis of the 1.85 Ga Sonakhan mafic dyke swarm, Bastar Craton, India

J.G. Shellnutt [a,*], K.R. Hari [b], A.C.-Y. Liao [a], S.W. Denyszyn [c], N. Vishwakarma [d], S.D. Deshmukh [e]

[a] National Taiwan Normal University, Department of Earth Science, 88 Tingzhou Road Section 4, Taipei 11677, Taiwan
[b] School of Studies in Geology and Water Resource Management, Pt. Ravishankar Shukla University, Raipur 492010, Chhattisgarh, India
[c] University of Western Australia, School of Earth Sciences, 35 Stirling Highway, 6009, Australia
[d] National Institute of Technology, Department of Applied Geology, Raipur, Chhattisgarh 492010, India
[e] Govt. V.Y.T.P.G. Autonomous College, Department of Geology, Durg, Chhattisgargh 491001, India

ARTICLE INFO

Article history:
Received 1 November 2018
Accepted 12 March 2019
Available online 15 March 2019

Keywords:
Mafic dyke swarm
Paleoproterozoic
Bastar Craton
Geochronology
Geochemistry

ABSTRACT

The NNW trending tholeiitic Sonakhan mafic dyke swarm of the Northern Bastar Craton is comprised of basalt to basaltic andesite (SiO_2 = 46.3 wt% to 55.3 wt%; Mg# = 37 to 70) dykes. A single basaltic dyke yielded a weighted-mean $^{207}Pb/^{206}Pb$ baddeleyite age of 1851.1 ± 2.6 Ma. The Sr and Nd isotopes ($^{87}Sr/^{86}Sr_i$ = 0.70396 to 0.70855; $\varepsilon_{Nd}(t) = -5.7$ to $+2.0$) are variable which is a consequence of crustal contamination. Trace element modeling suggests the dykes were likely derived by partial melting of a spinel-bearing mantle source. The Sonakhan dykes are 30 million years younger than the 1.88 Ga Bastar-Cuddapah dykes (Bastanar-Hampi swarm) of the southern and central Bastar Craton indicating they represent a distinct period of magmatism. However, much like the 1.88 Ga dykes, the Sonakhan dykes appear to be correlative with dykes from the Yilgarn Craton (Yalgoo dyke = 1854 ± 5 Ma) of Western Australia. The temporal and compositional similarity of the Sonakhan dykes with the Yalgoo dyke is evidence that they are petrologically related and may represent different branches of the same dyke swarm. The existence of two distinct Paleoproterozoic dyke swarms in the Bastar Craton that each have a correlative unit in the Yilgarn Craton is supportive of a link between India and Australia before 1.9 Ga. Moreover, it suggests that the break-up of India and Western Australia was protracted and lasted for at least 30 million years.

1. Introduction

Mafic dyke swarms are important geological features that can constrain the timing of continental break-up, mantle plume activity, and the paleolatitude of cratons that extend to the earliest Paleoproterozoic (Goldberg, 2010; Halls, 1982; Yale and Carpenter, 1998). The Archean crust of the Indian Shield has one of the highest concentrations of Precambrian mafic dyke swarms in the world (Murthy, 1995). However, only a few of the dyke swarms have been dated using high precision methods (Samal et al., 2019). Consequently, the correlation of dykes across India and with other cratons is difficult as it is currently based on bedrock cross-cutting relationships, mineralogy and geochemistry (Samal et al., 2019; Srivastava and Gautam, 2015). The majority of the dyke swarms across the Dharwar, Bastar and Singhbhum Cratons that have been dated using high precision U-Pb methods on baddeleyite (ZrO_2) or zircon ($ZrSiO_4$) yielded Paleoproterozoic (2.37 Ga to 1.89 Ga) ages but there is evidence that suggests there may be Meso- to Neoproterozoic dykes as well (Belica et al., 2014; Das et al., 2011; French et al., 2008; French and Heaman, 2010; Kumar et al., 2012; Pradhan et al., 2012; Radhakrishna et al., 1999; Rao et al., 2005; Samal et al., 2019; Shellnutt et al., 2018; Söderlund et al., 2018; Srivastava et al., 2018). Therefore, identifying and characterizing the mafic dykes of Peninsular India is pertinent for elucidating the extent of mafic magmatism that affected the Indian Shield over time as well as to clarify the constituents of proposed Archean to Paleoproterozoic (Ur, Columbia) and possibly younger (Rodinia) supercontinents (Mohanty, 2015a; Rogers and Santosh, 2004; Zhao et al., 2002).

There are at least three major Paleoproterozoic (2.5 Ga to 1.6 Ga) mafic dyke swarms within the Archean Bastar Craton of east-central India. The most well studied swarm is the Bastar-Cuddapah dyke swarm (BCDS) which is also referred to as the Bastanar swarm and considered to be a member of the Bastanar-Hampi large igneous province (French et al., 2008; Samal et al., 2019; Söderlund et al., 2018; Srivastava and Gautam, 2015). The BCDS was emplaced at ~1.88 Ga and extends across the Bastar and Dharwar Cratons and may have correlative dykes in the Yilgarn Craton of Western Australia (Belica et al., 2014; French et al., 2008; Liu et al., 2018; Shellnutt et al., 2018; Stark et al., 2018). The dykes and sills are primarily tholeiitic and have a radial orientation. Given the size, composition, and orientation, it is thought

* Corresponding author.
E-mail address: jgshelln@ntnu.edu.tw (J.G. Shellnutt).

https://doi.org/10.1016/j.lithos.2019.03.015

that the BCDS may be related to a mantle plume (Belica et al., 2014; French et al., 2008; Samal et al., 2019; Shellnutt et al., 2018). The NW trending boninite-norite (SiO_2 ≥ 52 wt%; MgO > 8 wt%) dykes of the 'BN' swarm were originally thought to be Neoarchean to Paleoproterozoic but Liao et al. (2019) has demonstrated that the boninitic dykes in the central Bastar Craton (Bhanupratappur) are ~2.37 Ga and correlative with dykes of the Bangalore-Karimnagar swarm of the Dharwar Craton (Samal et al., 2019; Söderlund et al., 2018; Srivastava and Gautam, 2015). The third Paleoproterozoic dyke swarm has not been dated. The dykes of 'BD1' swarm, located in the southern and central regions of the Bastar Craton, are tholeiitic with low Ti-Fe-HFSE (high field strength elements) and high-Mg and are interpreted, based on cross-cutting relationships, to be Meso- to Neoarchean in age (Samal et al., 2019; Srivastava and Gautam, 2015).

In the northern Bastar Craton, located south of the Chhattisgarh Basin (~100 km east of Raipur, Chhattisgarh) there is a series of NNW trending dykes. The dykes cross-cut the Archean basement rocks of the Bastar Craton (Baya gneiss) and the entire stratigraphy of the Sonakhan greenstone belt (SGB). The geological relationships in the region suggest that the dykes are no older than Paleoproterozoic as the SGB is considered to be Neoarchean in age (Manu Prasanth et al., 2018). The dykes are 50 m to 200 m wide, have doleritic textures and referred to as the Sonakhan dyke swarm (SDS) due to their spatial association with the SGB. Beyond the mineralogy and field relationships, very little is known about the SDS and they have not been correlated with any other dyke swarm of the Bastar Craton as its orientation is unique. Consequently, there are three possible geological scenarios for the SDS: 1) they are related to one of the three main Paleoproterozoic dyke swarms (Bangalore-Karimnagar, Bastanar, or BD1) of the Bastar Craton (Srivastava and Gautam, 2015), 2) they are a continuation of the subduction-related Paleo- to Neoproterozoic Newer Dolerites of the neighbouring Singhbhum Craton (Sengupta and Ray, 2012; Shankar et al., 2014), or 3) they are unrelated to any other known dyke swarm in Peninsular India. Thus, the characterization of the SDS may have significant implications for the post-cratonic evolution of the Indian Shield.

In this paper, we present a new high precision baddeleyite ID-TIMS (isotope dilution thermal ionization mass spectrometry) U-Pb age, whole rock geochemical data and Sr-Nd isotopes on a suite of dykes that cross-cut the Sonakhan greenstone belt and Archean basement rocks of the northern Bastar Craton of East-Central India. Our purpose is to constrain the petrogenetic evolution of the dykes and correlate them to other dyke swarms of the Bastar Craton and the Indian Shield. Moreover, we test hypotheses concerning the spatial and temporal relationship between the Bastar/Dharwar Cratons of India and the Yilgarn Craton of Western Australia during the Paleoproterozoic (Liu et al., 2018; Mohanty, 2012; Shellnutt et al., 2018; Söderlund et al., 2018; Stark et al., 2018).

2. Geological background

The Indian subcontinent preserves signatures of crustal recycling and juvenile additions during rifting–subduction–accretion and collision throughout geological time. Peninsular India is composed of several Archean cratonic nuclei which are linked together by Neoarchean and Paleoproterozoic orogenic belts (Naqvi and Rogers, 1987; Ramakrishnan and Vaidyanadhan, 2010; Santosh, 2012). Recent geological, geochronological and tectono-magmatic studies from the major cratons and intervening suture zones shows that this region is comprised of continental fragments that belonged to ancient and modern (e.g. Ur, Columbia, Rodinia, Gondwana) supercontinents (Rogers and Santosh, 2004). The ENE–WSW trending Central Indian Tectonic Zone, divides the Indian peninsula into northern and southern crustal blocks (Radhakrishna and Naqvi, 1986). The southern crustal blocks are composed of several Archean cratonic domains such as the Dharwar, Bastar, and Singhbhum, whereas the northern crustal block contains the Bundelkhand craton (Fig. 1a). The Dharwar, Bastar and Singhbhum cratons are juxtaposed along the NW-SE trending Pranihita Godavari and Mahanadi rift basins.

Being an important cratonic nucleus of the Peninsular Indian shield, the Bastar Craton occupies the key position in Central India (Sharma, 2009). It is bounded by the Central Indian Tectonic Zone in the north-west, Mahanadi Rift in the north-east, the Eastern Ghats mobile belt in the east to south-east and the Godavari Graben in the south-west (Meert et al., 2010). The Bastar Craton comprises a number of linear tectonic belts i.e., the Bengpal–Sukma Belt in the south, Kotri–Dongargarh Belt in the centre and north, the Amgaon Belt in the west and the Sasur–Chilipi Belt in the north and the Sonakhan Greenstone Belt in the north-eastern fringes (Fig. 1b; Ramakrishnan and Vaidyanadhan, 2010). Based upon the geochemical signatures of gneisses, granitoids and mafic dykes Mondal et al. (2006) suggested that the continental growth of the Bastar Craton took place during Precambrian time through multiphases of subduction and lithospheric extension or rifting processes. The Bengpal-Sukma belt contains the oldest group of rocks (Rajesh et al., 2009; Sarkar et al., 1993) and the basement rocks of the craton are dominated by tonalite–trondhjemite-granodiorite-gneisses (TTG) of 3.56 to 2.5 Ga (U-Pb zircon ages, Rajesh et al., 2009; Sarkar et al., 1993). The age of the granitoids range from 2.5 to 2.2 Ga (Rb-Sr isochron ages, Krishnamurthy et al., 1988) and major supracrustal sequences of the Bastar craton include Dongargarh, Sakoli and Sausar suites. The Dongargarh supracrustal sequence exhibit ages from 2463 to 2506 Ma (zircon U-Pb ages, Manikyamba et al., 2016). Several episodes of Neoarchean high-Mg mantle-derived magmatic imprints are found throughout the Bastar Craton (Samal et al., 2019).

The Sonakhan greenstone belt (SGB) which is located in the north-eastern part of the Bastar Craton represents a typical granite-greenstone belt that is comparable with the Dharwar Supergroup (Pascoe, 1973). It is encircled by the Mesoproterozoic Chhattisgarh basin and has a 'typical' Precambrian Granite-Greenstone Belt lithology. The Sonakhan greenstone belt, based on geological and lithological similarities, has been considered equivalent to Neoarchaean to Paleoproterozoic greenstone belts of the southern Bastar craton (Das et al., 1990). This interpretation is further corroborated by stratigraphic position as the greenstone belt underlies the Mesoproterozoic Chhattisgarh Supergroup (Das et al., 2009; Patranabis-Deb et al., 2007). Ghosh et al. (1995) presumed a Neoarchean age for this terrane based on whole rock Rb-Sr dating in meta-rhyolites. The Sonakhan terrane can be divided mainly into two groups namely the Sonakhan group and Bilari Group. The Baghmara formation and Arjuni formation are considered as the two main divisions of the Sonakhan Group. The Baghmara formation is mainly composed of massive metabasalts, pillow basalts, metagabbro, ignimbrite, rhyolite, felsic tuff, tremolite-actinolite schist, argillite, and ferruginous chert. Arjuni formation which overlies Baghmara formation mainly composed of Jonk conglomerates and banded iron formations (Das et al., 1990). The Baya gneissic complex is considered to be the basement of the Sonakhan terrane (Das et al., 1990). Pillow basalts and meta-basalts with relict pillow structure were documented from the lower part of the belt (Deshmukh et al., 2017; Mondal and Raza, 2009).

Deshmukh et al. (2017) reported the preliminary geochemistry of basalts and rhyolites from the Baghmara formation and proposed a supra-subduction zone tectonic setting for the SGB, whereas Mondal and Raza (2009) proposed a plume-arc interaction process for the origin of Sonakhan rocks. In a recent study, Manu Prasanth et al. (2018) proposed subduction of intraoceanic lithosphere and forearc magmatism in the Sonakhan area. Greenschist to lower amphibolite facies metamorphism have replaced the primary mineralogical and textural characteristics of the rocks present in the Sonakhan terrane. In addition, volcano-sedimentary successions of this terrane have undergone multiple stages of *syn*- and post-volcanic alteration, which are manifested as quartz veins, quartz fillings and epidotization.

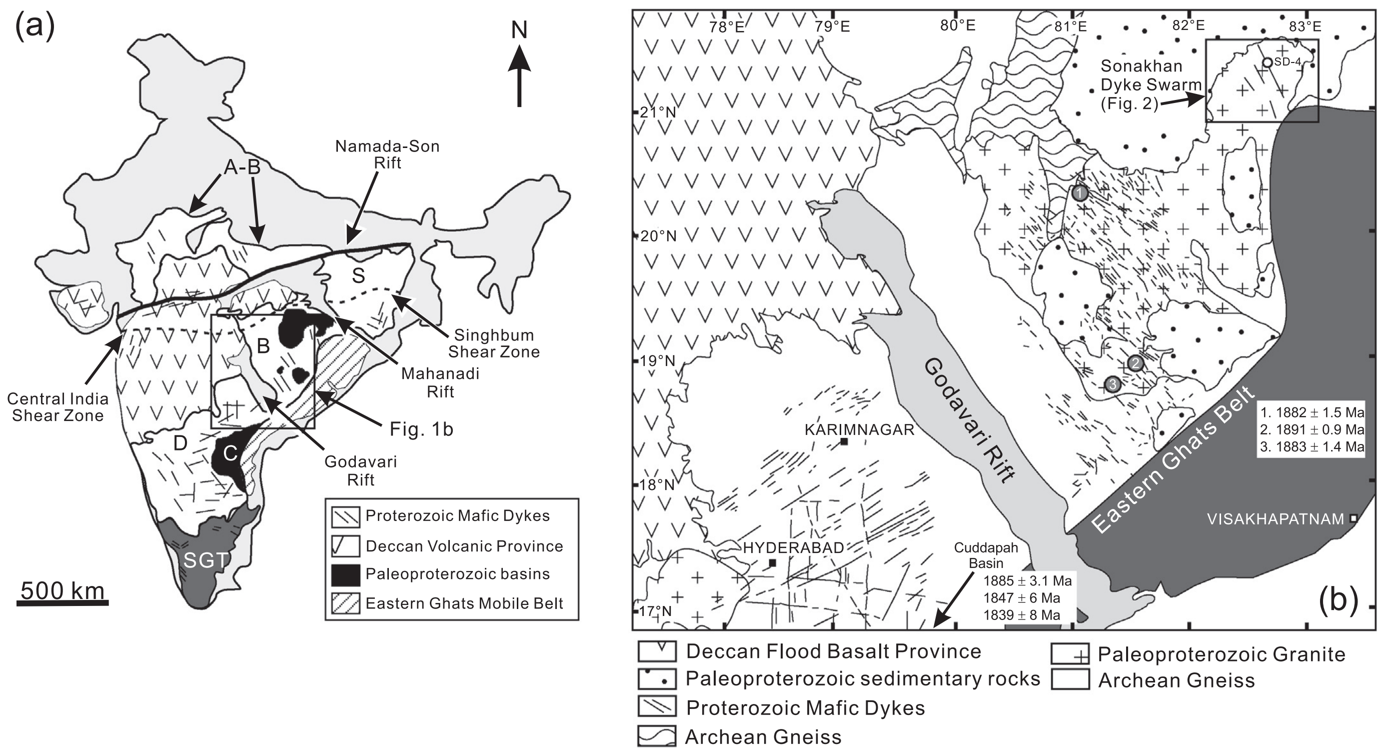

Fig. 1. (a) Cratonic divisions and regional geological structures of Peninsular India. D = Dharwar Craton, C = Cuddapah Basin, B = Bastar Craton, S = Singhbhum Craton, SGT = southern granulite terrane, A-B = Aravalli-Bundelkhand Craton. (b) Simplified regional geological map of the Bastar Craton and NE Dharwar Craton with location of the U/Pb geochronology sampling site (SD/4) of this study. Modified from French et al. (2008). Locations of 1.88 Ga Bastar-Cuddapah dykes (Bastanar-Hampi swarm) with high precision U/Pb dates are shown for reference (Belica et al., 2014; French et al., 2008; Shellnutt et al., 2018).

The Sonakhan dolerite dykes are trending in a NNW-SSE direction and vary from 100 m to >5 km in length and 30 m to 200 m in width (Figs. 2 and 3). The dykes are informally known as the Sonakhan dyke swarm but, based on the cross-cutting relationship, are likely to be younger and petrogenetically unrelated to the Sonakhan greenstone belt volcanic units. Exposure of the dykes is somewhat limited as the region is forested but 16 samples were collected for this study. From the hand specimens, most dykes were affected by greenschist facies metamorphism although there are a few dykes that appear to be fresh.

3. Petrography

The Sonakhan dykes are medium to coarse grained and variably altered ranging from minor (SD/4, SD/10, SD/12) to highly altered (other samples). The very altered (greenschist facies) rocks are comprised entirely or almost entirely of secondary minerals (hornblende, saussurite, chlorite). The least altered sample (SD/4) is comprised of clinopyroxene (~45–50 vol%) and plagioclase (~40 vol%) with minor (<10 vol%) amounts of Fe-Ti oxide minerals and accessory amounts (<1 vol%) of sulphide minerals and euhedral apatite. Many dykes retain their ophitic to sub-ophitic textures (Fig. 4). Clinopyroxene is the most abundant mineral and is subhedral to anhedral. The subhedral crystals tend to have angular crystal boundaries as they likely crystallized against lath-shaped plagioclase. The anhedral crystals are common but less abundant and have irregular boundaries. Some clinopyroxene crystals have minor alteration to hornblende along grain boundaries. The plagioclase crystals are typically euhedral to subhedral with lath-like shapes and interstitial to the clinopyroxene. In many cases the plagioclase crystals have patches of saussurrite alteration. The Fe-Ti oxide minerals, mostly magnetite (titanomagnetite) with subordinate ilmenite, have subhedral textures and interstitial to the plagioclase and clinopyroxene. Apatite is identified due to its high relief, unaltered appearance, and euhedral hexagonal shape. Acicular apatite was not observed.

4. Analytical methods

4.1. Geochronology

Baddeleyite crystals from sample SD/4 were separated using the Wilfley water-shaking table in a technique modified after Söderlund and Johansson (2002), and a pipette to remove a concentrate of small, dense, flat minerals off the Wilfley table. This yielded several small, euhedral baddeleyite grains and fragments. The weights of the baddeleyite crystals were calculated from measurements of photomicrographs and estimates of the third dimension. The weights are used to determine U concentration and do not contribute to the age calculation. The grains were cleaned with concentrated distilled HNO_3 and HCl and, due to their small size, no chemical separation methods were required. The samples were spiked with an in-house ^{205}Pb-^{235}U tracer solution for ID-TIMS analysis, and dissolution and equilibration of spiked single crystals was by vapour transfer of HF, using Teflon microcapsules in a Parr pressure vessel placed in a 220 °C oven for six days before transfer to outgassed, zone-refined rhenium single filaments with 5 μL of silicic acid gel. U-Pb isotope analyses were carried out at the University of Western Australia using a Thermo Triton T1 mass spectrometer, in peak-jumping mode using a secondary electron multiplier. Uranium was measured as an oxide (UO_2). Fractionation and deadtime were monitored using SRM 981 and SRM 982. Mass fractionation was 0.03 ± 0.06%/amu. Data were reduced and plotted using the software packages Tripoli (from CIRDLES.org) and Isoplot 4.15 (Ludwig, 2011). All uncertainties are reported at 2σ.

4.2. Major and trace elemental geochemistry

The rock specimens were initially cut into small chips using a diamond-bonded steel saw. The chips were then crushed using a steel jaw crusher. The crusher was cleaned using de-ionized water after each sample was processed. The samples were then pulverized to a fine powder (200 mesh) in an agate mill. Three grams of powder from

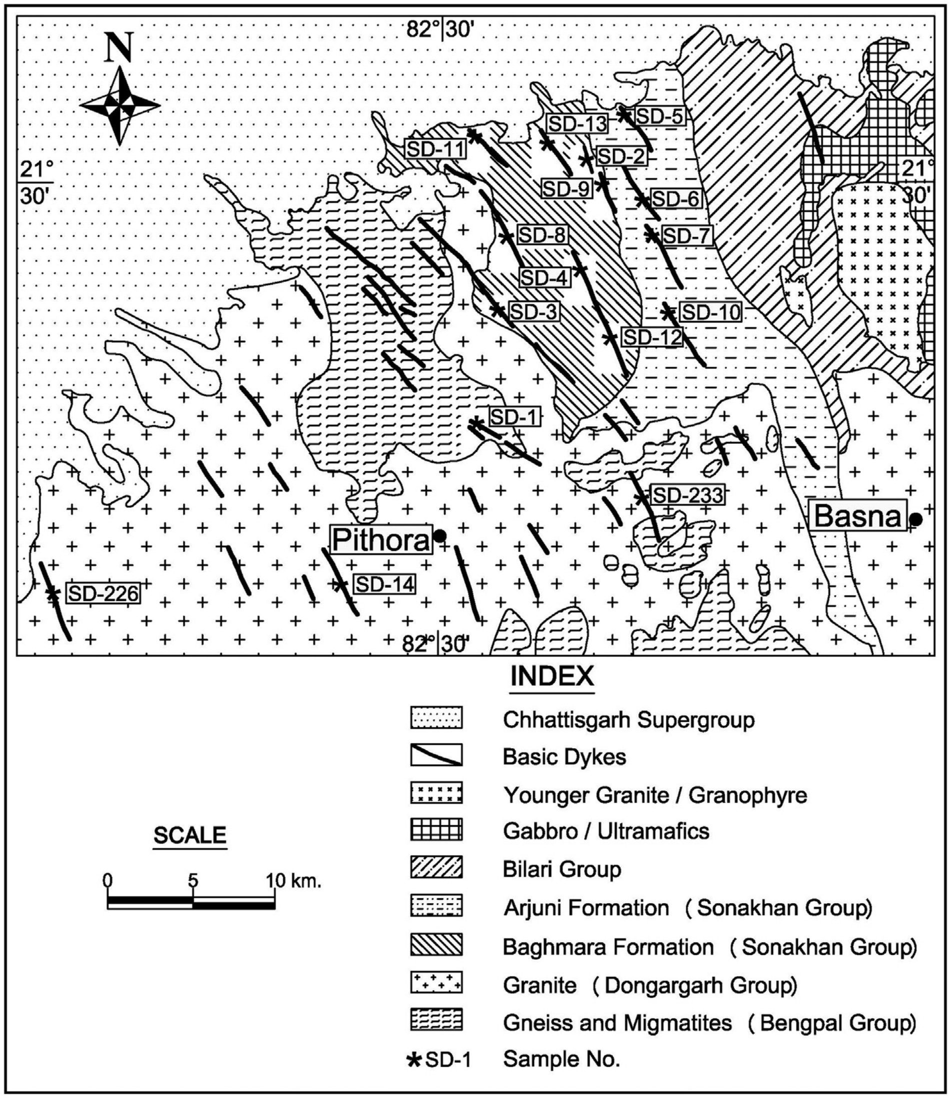

Fig. 2. Simplified geological map of the northern Bastar Craton showing the sample locations of this study and the distribution of the Sonakhan dykes.

each sample was baked and weighed, initially at 100 °C then 900 °C, to determine loss on ignition (LOI). Lithium metaborate was added to the oxidized samples after cooling from 900 °C and fused to produce a glass disc (Claisse M4 fluxer). The major oxide concentrations were determined by WD-XRFS using a PANalytical Axios mAX spectrometer at National Taiwan Normal University in Taipei. The measured standard reference material (AGV-2, BCR-2, BHVO-2, DNC-1, BIR-1) of the major elements are listed in Supplementary Table S2.

Trace elements were analyzed using an Agilent 7500cx inductively coupled plasma mass spectrometer (ICP-MS) at National Taiwan University, Taipei. Approximately 20 mg of rock powder from each sample was dissolved using a combination of HF, HNO_3 and HCl in a Teflon beaker. Each sample was heated with HF and HNO_3 in a closed beaker for 48 h and then dried. Subsequently, 2 mL of 6 N HCl were added and then left to dry. This step was repeated. Two mL of 1 N HCl was added to each sample after drying and then centrifuged. The supernatant was transferred to a new beaker. If solid residue was observed in the beaker then the procedure was repeated until complete dissolution. Samples were diluted using 2% HNO_3 and a Rh and Bi spike was added for the internal standard. The standard reference materials analyzed were BCR-2 (basalt), BHVO-2 (basalt), AGV-2 (andesite), and DNC-1 (dolerite). The accuracy of the measured standard reference material is generally better than ±5% for all elements.

4.3. Radiogenic isotopes

Strontium and Nd isotopes were measured at the Institute of Earth Sciences, Academia Sinica. A Finnigan MAT262Q thermal ionization mass spectrometer (TIMS) measured the Sr isotopes whereas a Thermo Fisher Scientific Triton Plus multicollector thermal ionization mass spectrometer measured the Nd isotopes. Approximately 100 mg of each sample powder was dissolved using HNO_3 and HF over a 48 h period which was followed by two rounds of 2 mL 6 N HCL and drying. Finally, 2 mL of 1 N HCl was added and the sample was centrifuged. If a solid residue was observed then the procedure was repeated. Sr and Nd were isolated from the remaining elements using chemical column separation methods. The first column used to isolate Sr and rare-earth elements (REEs) and contained 2.5 mL Bio-Rad AG50W-X8 cation exchange resin bed with grain size of 100 to 200 mesh. The Sr was further separated using a 1 mL resin bed of AG 50 W-X8 with 100 to 200 mesh grain size. Nd was concentrated using an 8 mL column with a 1 mL resin bed of Eichrom Ln (100–150 μ) that was covered by 0.1 mL of anion exchange resin bed (Dowex 1-X8, 100–200 mesh). The Sr samples plus H_3PO_4 were loaded on a single Re filament whereas the Nd samples plus H_3PO_4 were loaded on a double Re filament for analyses. The standard NBS987 Sr was measured 118 times between 2006 and 2017 and has a long-term value of 0.710248 ± 21. JMC Nd was measured

Fig. 3. Field photograph of dyke SD/3 striking 344° at 20 km milestone, Kasdol road (21°24′43.3″N, 82°32′08.7″E) near Pithora.

127 times between 2006 and 2016 and has a long-term value of 0.511816 ± 11.

5. Results

5.1. Geochronology

Six baddeleyite crystals were analyzed for U-Pb geochronology. Calculated weights are between 0.1 and 0.2 μg, with relatively low calculated U concentrations around 100 ppm. Th/U ratios are typically low in baddeleyite, and these analyses indicated Th/U ratios <0.05. The data are variably discordant (Fig. 5) with one analysis (#4 in Supplementary Table S1) at 5% discordance, indicating some small degree of Pb loss. The coherence of the $^{207}Pb/^{206}Pb$ ages of all data indicates any Pb loss was recent, and supports our interpretation of the weighted-mean $^{207}Pb/^{206}Pb$ age representing the magmatic emplacement age of the dyke. The weighted-mean $^{207}Pb/^{206}Pb$ age of all six analyses is 1851.1 ± 2.6 Ma (2σ, MSWD = 1.5, N = 6).

5.2. Whole rock geochemistry

The Sonakhan dykes are tholeiitic and have SiO_2 ranging from 46.3 wt% to 55.2 wt% which corresponds to basalt and basaltic andesite (Supplementary Table S2; Fig. 6a). The Mg# [(Mg^{2+}/(Mg^{2+}+Fe^{2+}))*100] varies from ~37 to ~70 but there appears to be two groups of dykes (Fig. 6b). The high Mg# (>54) group has MgO > 6.8 wt% and Fe_2O_3t < 13 wt% whereas the low Mg# (<45) has MgO < 6.2 wt% and Fe_2O_3t > 14.5 wt%. The CaO (8.2 wt% to 11.5 wt%) and Al_2O_3 (9.3 wt% to 15.6 wt%) contents of both groups are similar but Al_2O_3 tends to be lower in the high Mg# group that has high SiO_2 (Fig. 6c). Moreover, the high Mg# samples also have lower TiO_2 (<1.1 wt%) than the rocks with lower Mg# (TiO_2 > 1.1 wt%) (Fig. 6d). The MnO and P_2O_5 contents are generally higher in the low Mg# samples. The total alkalis (Na_2O and K_2O) have a large range (Na_2O + K_2O = 1.8 wt% to 4.4 wt%) in the high Mg# samples but it encompasses the range of the low Mg# samples (Na_2O + K_2O = 2.5 wt% to 3.5 wt%). The loss on ignition (LOI) for all samples ranges from 0.48 wt% to 2.58 wt%. All samples are quartz, diopside and hypersthene normative except SD/9, SD/11 and SD/14 (high Mg#) which are olivine, diopside and hypersthene normative.

The transition metals (Sc, V, Zn, and Co) are relatively uniform although Ni (59–424 ppm), Cr (45–1073 ppm), and Cu (70–255 ppm) are quite variable (Fig. 6e-f). Both the high field strength elements (Zr = 41–155 ppm, Nb = 1.7–12.6 ppm, Hf = 1.19–4.10 ppm, Ta = 0.11–0.83 ppm, Th = 0.26–5.10 ppm, U = 0.10–1.49) and large ion lithophile elements (Cs = 0.16–5.04 ppm; Rb = 4.2–55.5 ppm; Ba = 28–571 ppm; Sr = 120–362 ppm) are variable but in most cases the variability is due to the anomalous values from samples SD/1, SD/2, SD/4, SD/5 and SD/6. The primitive mantle normalized incompatible trace element patterns are broadly similar between the high Mg# and low Mg# groups as they are parallel and have enriched LILE and depletions of Nb-Ta (Fig. 7a). The chondrite normalized REE patterns range from light-rare earth element (LREE) depleted to enriched (La/Yb_N = 0.9 to 9.2; Gd/Yb_N = 1.0

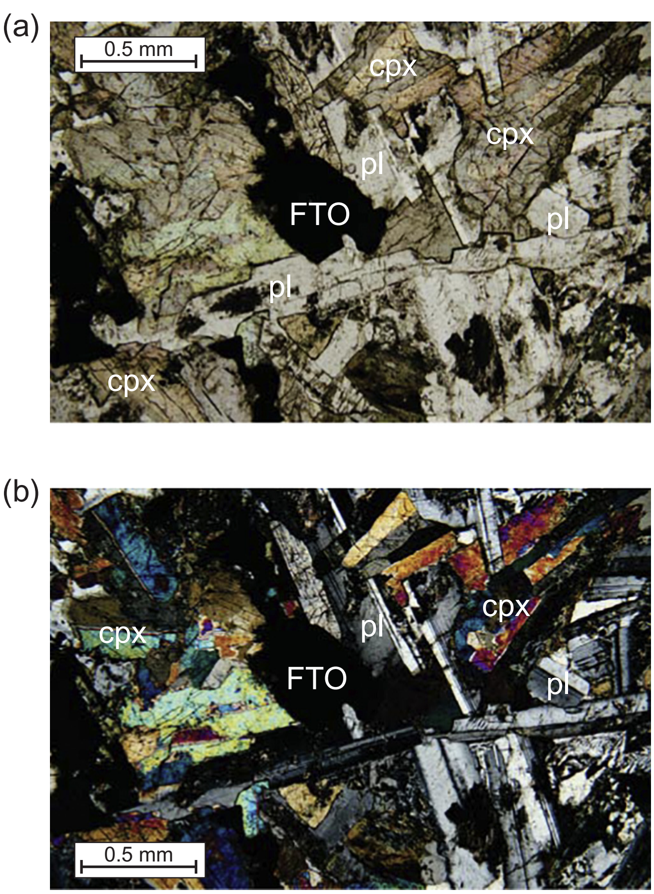

Fig. 4. Photomicrograph of sample SD/4 in (a) plane polarized and (b) cross-polarized light. cpx = clinopyroxene, pl = plagioclase, FTO = Fe-Ti oxide minerals.

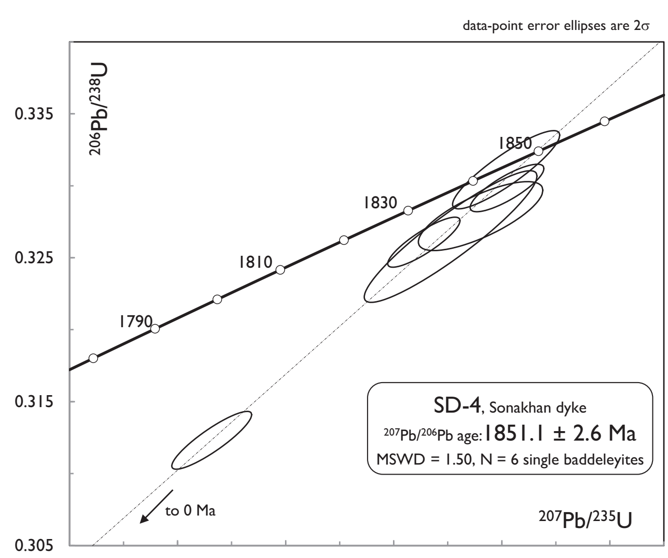

Fig. 5. Concordia plot of baddeleyite U-Pb TIMS data for sample SD/4.

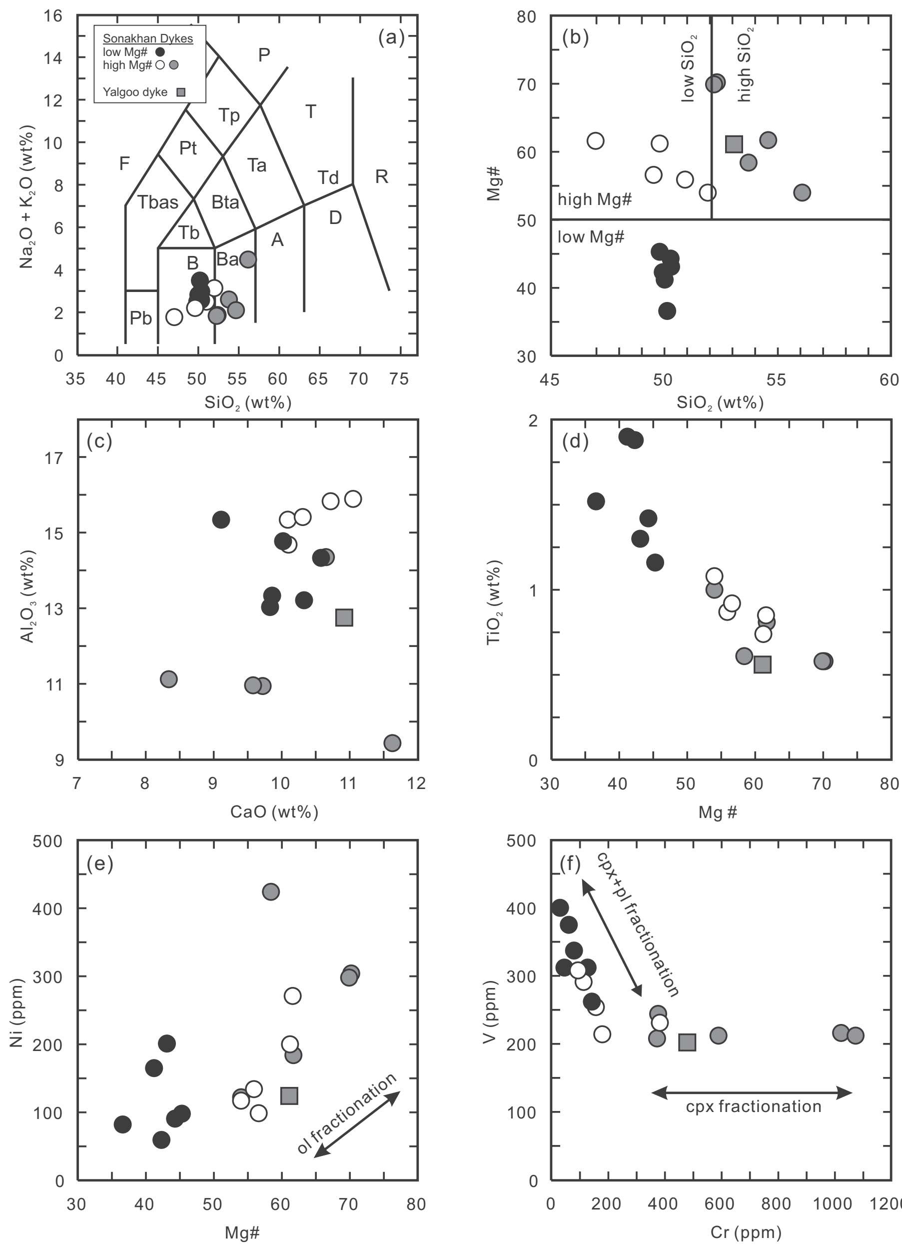

Fig. 6. Major and trace element compositions of the Sonakhan dykes. (a) $Na_2O + K_2O$ (wt%) versus SiO_2 (wt%) classification of LeBas et al. (1986). F = foidite, Pb = picrobasalt, B = basalt, Ba = basaltic andesite, A = andesite, D = dacite, R = rhyolite, TB = tephrite or basanite, PT = phonotephrite, Tp = tephriphonolite, P = phonolite, T = tachyte, Tb = trachybasalt, Bta = basaltic trachyandesite, Ta = trachyandesite, Td = tachydacite. (b) Mg# [$(Mg^{2+}/(Mg^{2+}+Fe^{2+}))$*100] versus SiO_2 (wt%) showing the division of the rocks based on Mg# and 'higher' and 'lower' SiO_2 groups. (c) Al_2O_3 (wt%) versus CaO (wt%) showing lower Al_2O_3 contents of the 'high' SiO_2 dykes. (d) TiO_2 (wt%) versus Mg# showing the higher concentration of TiO_2 within the low Mg# dykes. (d) Ni (ppm) versus Mg#. The positive relationship may be indicative of olivine fractionation. (f) V (ppm) versus Cr (ppm). The flat trend probably represents fractionation of clinopyroxene whereas the increase of V may be due to fractionation of clinopyroxene and plagioclase. Yalgoo dyke composition from Ameen and Wilde (2006).

to 2.1) with some bearing a resemblance to N-MORB (SD/7, SD/8 and SD/11) whereas others are more similar to *E*-MORB and ocean-island basalt. The rocks do not display distinct Eu-anomalies as all samples have Eu/Eu* values between 0.86 and 1.03 (Fig. 7b).

5.3. Sr-Nd isotopic geochemistry

The initial Sr-Nd isotope ratios are calculated using the 1850 Ma U/Pb age of sample SD/4. The initial $^{87}Sr/^{86}Sr$ (ISr) ratio ranges from 0.698005 to 0.708547 (Supplementary Table S3). Sample SD/12 has a low initial ratio (<0.7000) suggesting that it was affected by element mobility. The remaining samples have ISr values from 0.703960 to 0.708547. The initial $^{143}Nd/^{144}Nd$ ratios range from 0.509953 to 0.510344 and correspond to $\varepsilon_{Nd}(t)$ values of −5.7 to +2.0 (Fig. 8). The meaningful ($^{147}Sm/^{144}Nd < 0.165$) depleted-mantle model ages (T_{DM}) range from 2569 Ma to 2886 Ma.

6. Discussion

6.1. Petrogenesis of the Sonakhan dykes

6.1.1. Fractional crystallization within the Sonakhan dykes

The chemical variability, specifically the low Mg# (<40) and the lower Ni (≤ 200 ppm) contents, observed within some Sonakhan dykes suggests their parental magmas likely experienced fractional crystallization at some point during their emplacement. Even the rocks with higher Mg# (>60) tend have lower CaO (<11 wt%) content then primitive basalt suggesting they are not primary magmas

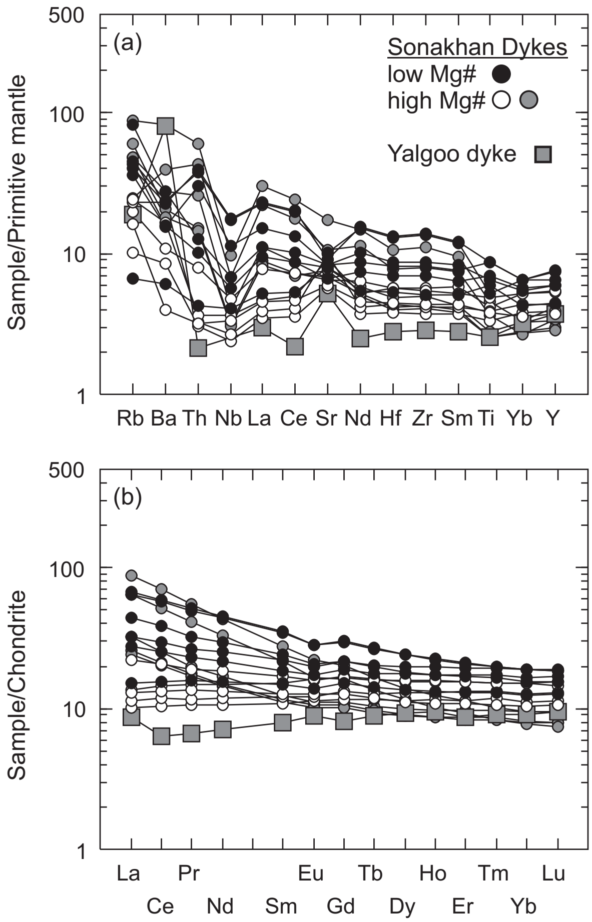

Fig. 7. (a) Primitive mantle normalized incompatible element plot and (b) chondrite normalized rare earth element plot of the Sonakhan dykes from this study. Samples are normalized to the values of Sun and McDonough (1989). Yalgoo dyke composition from Ameen and Wilde (2006).

(Herzberg et al., 2007). Moreover the decreasing MgO and Fe_2O_3t and increasing Na_2O and K_2O with respect to SiO_2 indicates silicate mineral (olivine, pyroxene, plagioclase) fractionation may explain some of the chemical variability amongst the dykes.

Fractional crystallization of major rock forming silicate minerals in mafic magmatic systems can be modeled using Pearce element ratios

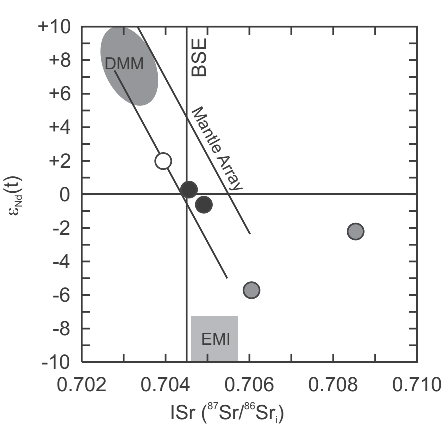

Fig. 8. ε_{Nd}(t) versus initial $^{87}Sr/^{86}Sr$ ratios (ISr) of the Sonakhan dykes. Fields of depleted mid-ocean-ridge basalt mantle (DMM), the mantle array, and enriched mantle I (EMI) are shown with the bulk silicate earth (BSE) evolution lines are shown for comparison. Symbols are the same as Fig. 6.

(PER). PER are calculated using major element data to evaluate the possible effects of olivine, pyroxene and plagioclase fractionation (Nicholls and Russell, 2016). The major element components are arranged according to the stoichiometric proportions of the possible fractionating silicate minerals (olivine, clinopyroxene, plagioclase) with respect to a conserved element. A conserved element is one that is not a major component (e.g. Ti, P, K, Zr) of one or more of the fractionating minerals (e.g. olivine, clinopyroxene, plagioclase). PER were designed to minimize the effects of the Chayes' closure problem and to better evaluate if fractionation of a specific mineral or groups of minerals occurred. Potassium meets the requirement of a conserved element for the Sonakhan dykes and the PER indicate that olivine and plagioclase fractionated and possibly clinopyroxene (Fig. 9). Although PER can identify the effects of silicate mineral fractionation, they cannot give the proportions of the minerals fractionation and the relative timing of fractionation. To further evaluate the extent of fractionation we use the software MELTS (Smith and Asimow, 2005).

Two fractionation models were run using the same starting composition but with different relative oxidation states. Both models use sample SD/9 as the starting composition with initial water content of 1.5 wt % and pressure of 0.5 kbar (0.05 GPa) however one model used a relative oxidation state (fO_2) equal to NNO -1 (nickel-nickel-oxide) whereas the second model used a value of NNO -2 (Supplementary Table S4). Sample SD/9 was selected as the starting matieral because it has low SiO_2, high Mg# (61), high MgO (10.40 wt%), high Ni content (271 ppm), and is olivine normative.

The liquid evolution compositions of both models (model 1 = white circles; model 2 = black circles), at 10 °C intervals, are shown in Fig. 10 (Table S5). The results support the Pearce element ratio calculations and indicate that the compositional variability of the dykes may be explained by fractional crystallization of olivine, plagioclase and clinopyroxene. Model 1 (NNO -1) calculates olivine ($Fo_{85.5}$)

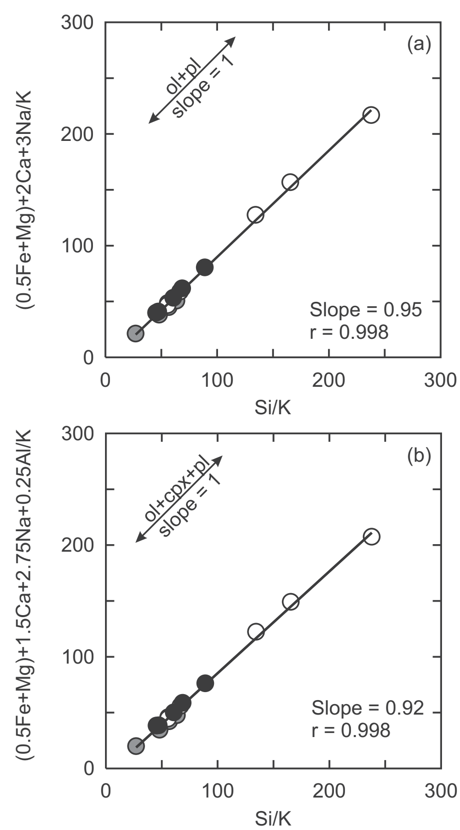

Fig. 9. Pearce element ratio plots of (a) olivine + plagioclase fractionation and (b) olivine + clinopyroxene + plagioclase fractionation. ol = olivine, pl = plagioclase, cpx = clinopyroxene. r = correlation coefficient.

crystallization at 1230 °C followed by plagioclase (An_{90}) at 1130 °C, clinopyroxene ($Wo_{44}En_{43}Fs_{13}$) at 1100 °C and finally spinel (Ti-rich magnetite) at 1050 °C. The compositional range of the dykes is produced as the liquid reaches 1030 °C (olivine = $Fo_{50.8}$; plagioclase = An_{74}, clinopyroxene = $Wo_{38}En_{38}Fs_{24}$) after which ~68% of the parental magma has crystallized.

Model 2 was run at a lower relative oxidation (fO_2 = NNO -2) state in order to reach the high TiO_2 values of samples SD/4 and SD/12 (Table S6). Model 2 calculates olivine ($Fo_{84.8}$) crystallization at 1240 °C followed by plagioclase (An_{90}) at 1130 °C, clinopyroxene ($Wo_{45}En_{44}Fs_{11}$) at 1110 °C and finally spinel (Ti-rich magnetite) at 1040 °C. The compositional range of the dykes is produced as the liquid reaches 1010 °C (olivine = $Fo_{33.6}$; plagioclase = An_{71}, clinopyroxene = $Wo_{42}En_{31}Fs_{27}$) after which ~74% of the parental magmas has crystallized. Most importantly, the TiO_2 peaks at ~1.8 wt% in model 2 which is similar to the high-Ti dykes (~1.9 wt%).

It is very likely that the primary magmas of the Sonakhan dykes had already experienced fractionation of olivine with or without a Ca-rich silicate (plagioclase or clinopyroxene) mineral before reaching shallow levels of the crust. The implication is that the basaltic magma differentiated at two stages. The first stage of fractionation was probably located near the crust-mantle boundary whereas the second stage occurred in the upper crust either within a magma chamber and/or a conduit during transport to the surface. The MELTS models and PER are mutually consistent in that they both indicate the chemical variability of the dykes is, in part, related to fractional crystallization of olivine, plagioclase

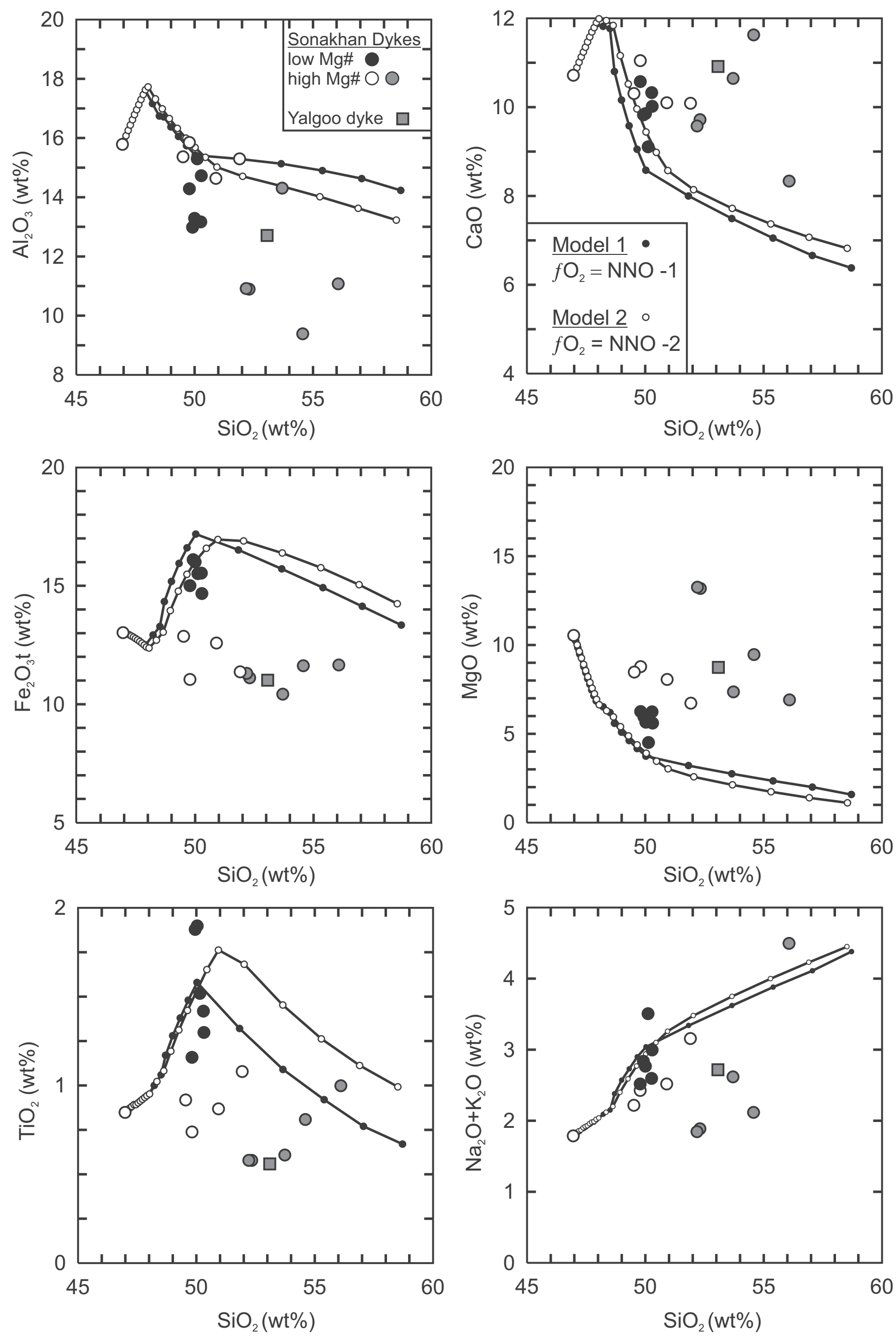

Fig. 10. Results of MELTS modeling showing the major element liquid compositional evolution curves of the Sonakhan dykes using the starting compositions found in Supplementary Table S4. Model 1 (black circles) and model 2 (white circles) shows fractional crystallization curves using different initial relative oxidation states. The dots (black, white) represent liquid compositions at 10 °C intervals. The composition of the Yalgoo dyke is reported by Ameen and Wilde (2006).

and clinopyroxene probably at shallow levels of the crust. Titanomagnetite likely played a minor role (~1.5% of the total assemblage) near the end of fractionation. There are a few samples that have higher SiO_2 (>52 wt%) and lower Al_2O_3 (<11 wt%) which the models cannot reproduce suggesting there could be an additional magmatic processes (e.g. crustal contamination) that affected individual dykes.

6.1.2. Crustal contamination

Based on the major element compositions and the MELTS modeling it is clear that there are a number of high Mg# samples (SD/1, SD/2, SD/3, SD/5, SD/6) that have high normalized SiO_2 (>52 wt%) and low normalized Al_2O_3 (<11.5 wt%) contents with respect to other high Mg# samples (Fig. 5b and c). The paradox of high Mg# and high SiO_2 suggests that crystal fractionation may not be the only process that contributed to the chemical variability of the dykes. It is possible that some dykes were contaminated by crustal material (melts?) during emplacement.

The primitive mantle normalized plots show that nearly all samples have depletion of Nb and Ta but, perhaps more importantly there is a trend of increasing Th/Nb_{PM} ratio with a decreasing Nb/U ratio (Fig. 11a). The trend implies that there was contamination within the dyke swarm as the data trend from high values toward the composition of average upper crust ($Th/Nb_{PM} \approx$ ~7; Nb/U $\approx$ 5). There are a number of other trace element ratios that suggest the high Mg# and high SiO_2 samples were contaminated. The Th/Yb ratios increase vertically with the high SiO_2 samples indicating the possibility of crustal contamination (Fig. 11b). Furthermore, the La/Nb ratio increases from 1.2–1.6 in the low SiO_2 rocks to 2.5–3.0 in the high SiO_2 rocks. The Zr/Y ratio with respect to Zr shows a non-horizontal trend suggesting that the ratio variability is not just related to fractional crystallization (Fig. 11c). Finally, the increase in the Dy/Yb ratio at relatively constant Dy/Dy* values suggests enriched crustal material contaminated some dykes (Fig. 11d). Consistently, the high Mg# and high SiO_2 samples demonstrate compelling evidence in favour of crustal contamination. In contrast the high Mg# and low SiO_2 samples (SD/7, SD/8, SD/9, SD/11, SD/14) have less variability (lower Th/Nb_{PM}, higher Nb/U, lower La/Nb, lower Th/Yb) in their trace element ratios implying that they were minimally contaminated, if at all (Fig. 11).

From the perspective of the Sr-Nd isotopes, the high Mg# and high SiO_2 samples (SD/2, SD/6) have higher initial $^{87}Sr/^{86}Sr$ ratios (0.70606 to 0.70855) and lower εNd(t) values (−5.7 to −2.2) than the high Mg# and low SiO_2 rocks (SD/8; ISr = 0.70396; εNd(t) = +2.0). The isotopic trend, much like the trace element ratio trends, is consistent with isotopic enrichment via crustal contamination. Isotopic modeling using Archean basement rocks of the Bastar Craton as the 'crust' end-member and the 'least contaminated' high Mg# dyke (SD/8) as the 'pristine' end-member indicates that ~15% contamination could increase the initial $^{87}Sr/^{86}Sr$ ratio from ~0.7040 to ~0.7088 (Table S6). Moreover, the amount of contamination, using the reported Bastar gneiss composition, would likely increase the bulk SiO_2 (~50 wt%) and Sr (176 ppm) content to the values closer to the most contaminated (SD/6) dyke (SiO_2 = ~55 wt%; Sr = 362 ppm). However, it is likely that the crustal melt was more silicic than the bulk compositions used for isotopic modeling (i.e. SiO_2 > 69 wt%). The implication is that contamination probably occurred either after or concomitant with crystal fractionation (assimilation fractional crystallization). In other words, the

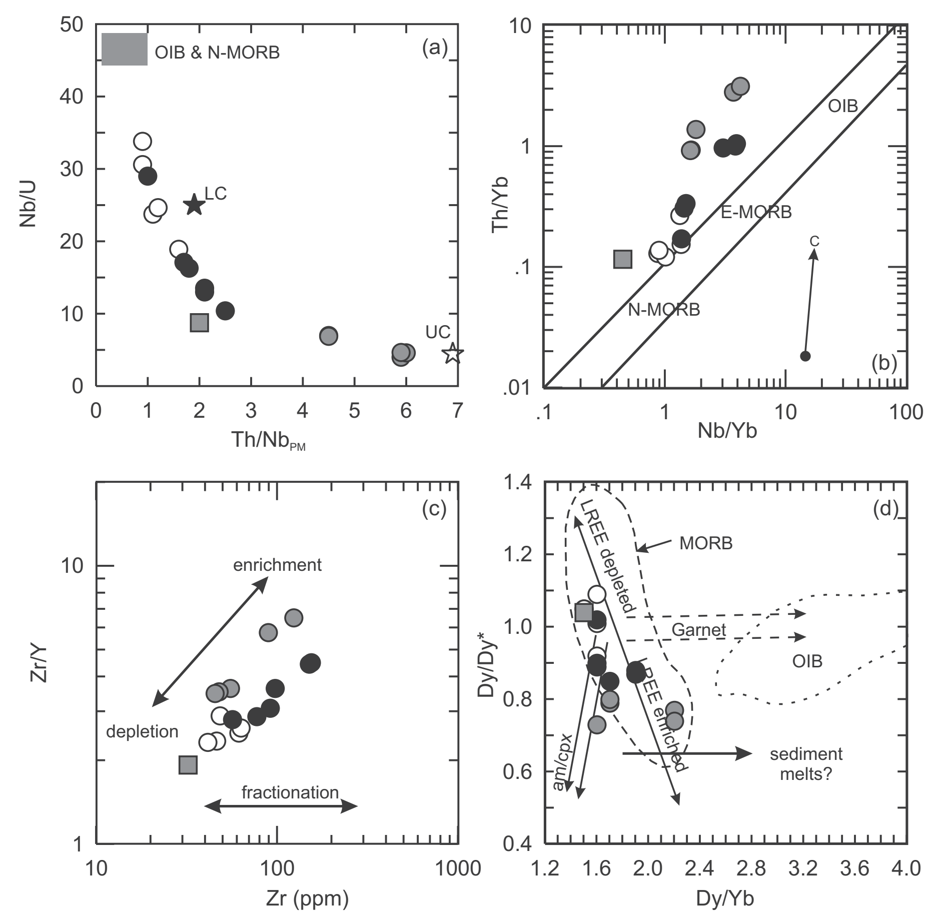

Fig. 11. (a) Nb/U versus Th/Nb_{PM} of the Sonakhan dykes with the compositions of average lower (LC) and upper (UC) continent crust and the range for ocean island basalt (OIB) and normal mid-ocean ridge basalt (N-MORB). PM = primitive mantle (Rudnick and Gao, 2003; Sun and McDonough, 1989). (b) Th/Yb versus Nb/Yb showing an enrichment trend indicative of crust contamination (Pearce, 2008). (c) Zr/Y versus Zr (ppm) (Pearce and Norry, 1979). (d) Dy/Dy* versus Dy/Yb (Davidson et al., 2013). Yalgoo dyke composition from Ameen and Wilde (2006).

petrogenesis of the most contaminated sample probably occurred as fractionation (olivine, plagioclase, clinopyroxene) increased the SiO_2 and Sr concentrations to elevated levels (e.g. SiO_2 = ~54 wt%, Sr = 300 ppm) which were then mixed with highly silicic crustal melts (i.e. $SiO_2 \approx 75$ wt%).

6.1.3. Mantle source characteristics

The high Mg# and low SiO_2 dykes (SD/7, SD/8, SD/9, SD/11, SD/14) are the best examples of the least contaminated and most 'primitive' compositions found in this study and therefore are better suited to constrain the mantle source characteristics of the Sonakhan dyke swarm. In addition to high Mg#, high Ni contents, and low SiO_2, the 'primitive dykes' have relatively low chondrite normalized La/Yb ratios (0.9 to 1.5) that are more similar to N-MORB/*E*-MORB than the LREE-enriched (La/Yb_N = 3.4 to 9.2) compositions of the 'contaminated' samples (Fig. 7b). The slightly depleted to relatively flat chondrite normalized REE patterns suggest that the mantle source could be similar to depleted-MORB mantle but the Sr-Nd isotopes ($^{87}Sr/^{86}Sr_{initial}$ = 0.7045; $\varepsilon Nd_{(1.85\ Ga)} = 0 \pm 1$) are more chondritic than radiogenic ($^{87}Sr/^{86}Sr_{initial}$ = 0.7040; $\varepsilon Nd_{(1.85\ Ga)} = +5$) and the rocks have Dy/Dy* (0.92 to 1.09) values that are more similar to primitive (Dy/Dy* $\approx$ 1) mantle than depleted (Dy/Dy* $\approx$ 1.75) mantle (Davidson et al., 2013). The implication is that the mantle source was not depleted but could be lithospheric or conceivably a mantle plume-type source (Cagney et al., 2016; Workman and Hart, 2005).

Batch melting trace element modeling indicates that most of the incompatible trace element concentrations of the dykes can be replicated by 12% to 18% partial melting of a spinel lherzolite (olivine = 55%, orthopyroxene 25%, clinopyroxene = 15%, spinel = 5%) assuming an initial composition similar to primitive mantle (Table S7). There are some elements that do not match the modeled concentrations very well but it is likely that Ti, Ba, Sr and Rb increased in the residual dyke liquid compositions during fractionation of olivine. As previously mentioned the dyke magmas likely experienced crystal fractionation and are not 'primary' compositions. The low Dy/Yb (1.5 to 1.6) and Sm/Yb_{PM} (1.0 to 1.1) values suggest garnet was not a residual phase within the source after melting (Davidson et al., 2013). It is possible that all garnet in the source was consumed during melting as the trace element modeling indicates relatively high amounts of melting are required to replicate the dyke compositions. However, the low Tb/Yb_N values (1.0 to 1.1) at FeO normalized to 8 wt% MgO (Fe_8 = 9.5 wt% to 11.2 wt%) suggest that melting of the mantle source occurred outside (structurally above) of the garnet stability field (Wang et al., 2002).

The mantle source for the Sonakhan dyke swarm was isotopically chondritic as the Sr-Nd isotopes for the uncontaminated samples are similar to bulk silicate earth. The bulk composition of the source was probably similar to primitive mantle as it can replicate the chondrite normalized REE patterns of the rocks. At the moment there is not enough evidence to support the hypothesis that the primary magmas of the dykes were derived from a mantle source within the garnet stability field. Therefore it is unlikely the parental magmas of the dykes are related to deep seated mantle upwelling. Additionally, the Sonakhan dyke swarm is the only known dyke swarm of the Indian Shield that was emplaced at 1.85 Ga suggesting that a geographically extensive radiating swarm may not exist and that it was a comparatively smaller magmatic event.

6.1.4. Emplacement of the Sonakhan dyke swarm

The SDS was likely emplaced during a period of tensional plate stress within the northern Bastar Craton. Dyke swarms of similar size as the SDS are often but not exclusively considered to be related to continental break-up and/or a mantle plume (Ernst, 2014; Ernst and Bleeker, 2010; Shellnutt and MacRae, 2012). The whole rock geochemistry indicates that crystal fractionation and crustal contamination are the main factors that explain the chemical variability of the dykes. Furthermore, trace element modeling and the Sr-Nd isotopes suggests high degrees (10% to 20%) of partial melting of a spinel-bearing lherzolite source likely produced the initial primary magmas. In this section we outline a sequential emplacement model of the SDS.

Melting of the mantle source was initiated as rifting developed within the northern Bastar Craton. The primary melts of the most primitive dykes likely experienced early crystal fractionation of olivine during melt transfer into the crust. It is possible that clinopyroxene fractionated early as well because samples SD/9 and SD/11, the most 'primitive' compositions, have relatively low CaO (~10.6 wt%) content and variable Cr (179 and 382 ppm) content. It is uncertain if early crystal fractionation occurred within a 'lower crust hot zone' or if it occurred during magma transport through the crust. Some of the 'primitive dykes' were emplaced within the upper crust whereas others stalled and fractionated olivine, plagioclase and clinopyroxene. The second stage of crystal fractionation produced the low Mg# magmas which were then injected into the overlying crust.

Contamination of the Sonakhan dykes is most acute within the high Mg# dykes. The high Mg#, high SiO_2 dykes have higher Th/Nb_{PM} and low Nb/U ratios than the other dykes. The implication is that contamination was more severe within the 'primitive' dykes. Based on the MELTS models, the liquidus temperature of the uncontaminated high Mg# dykes, as represented by sample SD/9, is ~1230 °C. Such a high temperature is sufficient to melt most supracrustal (0.5 kbar) lithologies (Clark et al., 2011; Sawyer et al., 2011). In comparison, the liquid temperature range that can yield liquid compositions similar to the low Mg# dykes is 1100 °C to 1050 °C. Consequently, by virtue of their high temperature, the high Mg# dykes were probably more likely to induce melting of the crust and thereby have an increased probability of assimilating crustal melt during crystal fractionation. Furthermore, it is probable that the dykes fed volcanic eruptions and that there are/were basalts that can be compositionally correlated with the dykes.

6.2. Correlation of the Sonakhan dykes with tectonomagmatic events in the Bastar Craton

Age spectra of detrital zircons from Mesoproterozoic sedimentary rocks of the Bastar Craton indicate there was a major crust building episode in the region at ~1.85 Ga (Mohanty, 2015b). Geological, geochemical and geochronological evidence indicates there were at least two tectonomagmatic episodes during the interval from 1.9 Ga to 1.8 Ga (Mishra and Kumar, 2014; Mohanty, 2015b; Saha and Mazumder, 2012). Mohanty (2015b) outlines the two major tectonic events in the Bastar Craton as: 1) the second phase (1b) of the initial stage of the Satpura Orogeny (1.95 Ga to 1.90 Ga) which is characterized by high-grade metamorphism and migmatization and was accompanied by granitic magmatism, and 2) the emplacement of the BCDS at 1.88 Ga. The Chhattisgarh Supergroup (sandstone, shale, conglomerates) was deposited at ~1.45 Ga and uncomforambly overlies the Paleoproterozoic basement rocks (Dhang and Patranabis-Deb, 2011).

The BCDS(1.88 Ga), although compositionally similar to the Sonakhan dykes, is 30 million years older than the SDS(1.85 Ga) indicating that they may not be petrogenetically related although they could be broadly related to the same regional rifting regime that extended across India(Shellnutt et al., 2018). There are mafic dykes that have similar ages as the SDS but they are primarily located in southern India. There is a mafic dyke near Dharmapuri (~1100 km south of the SDS), within the South India Granulite Terrane, that has a plagioclase $^{40}Ar/^{39}Ar$ age of 1855 ± 9 Ma but the high temperature spectrum did not yield a well define plateau (Radhakrishna et al., 1999). Analysis of two single zircon grains from a dyke in the Kunigal region (~150 km northwest of Dharmapuri) in the Dharwar Craton yielded $^{207}Pb/^{206}Pb$ ages of 1847 ± 6 Ma and 1839 ± 8 Ma but the dyke is interpreted to be a member of the BCDS based on its similar paleomagnetic directions (Belica et al., 2014). Furthermore, Sheppard

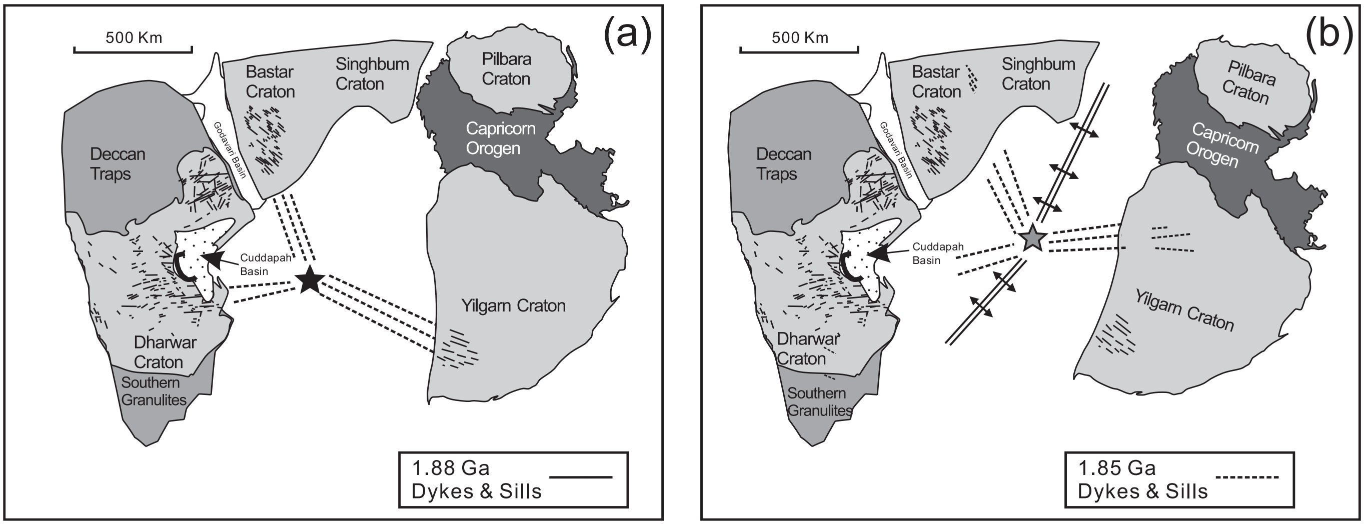

Fig. 12. Conceptual model of rift propagation from 1.88 Ga to 1.85 Ga. The original reconfiguration is based on Stark et al. (2018). (a) The initial rift and magmatism begin at ~1.88 Ga as Peninsular India and Western Australia are proximal. (b) Extension continues and rift propagates NE-ward and the younger dykes are emplaced at ~1.85 Ga. There is uncertainty regarding the precise age of Paleoproterozoic dykes from southern India but are shown for geographic context.

et al. (2017) dated felsic tuff within the upper part of the Tadpatri Formation that yielded weighted mean zircon SHRIMP ^{207}Pb/^{206}Pb ages of 1864 ± 13 Ma and 1858 ± 16 Ma (1862 ± 9 Ma combined age) and suggests that it may be amongst the youngest volcanic cycles in the Cuddapah Basin that spanned ~30 million years. Thus, it is possible that the SDS is a younger member of a larger magmatic province that spanned Peninsular India.

To the north of the Bastar Craton, rocks from the Mahakoshal fold belt and Bunkelkhand Craton record a deformation event at ~1.80 Ga which was likely preceded by the eruption of flood basalts (Gwalior Series lavas), emplacement of associated mafic dykes, and "post-tectonic" granites (Mohanty, 2015b; Saha and Mazumder, 2012). However the only available date of the basalt is an Rb-Sr isochron age of 1815 ± 200 Ma (Crawford and Compston, 1970; Rao et al., 2005). The Tamkhan and Barambara post-tectonic granites in the Mahakoshal fold belt have Rb-Sr isochron ages of ~1865 and ~1800 Ma respectively but there is uncertainty regarding their true correlation due to the precision of the dates (Sarkar et al., 1998). The deposition of the Mahakoshal Group sediments (shallow marine to deep shelf) are consistent with rifting and broadly contemporaneous with the SDS but their association (temporal and spatial) requires more evidence (Saha and Mazumder, 2012). Farther to the west in the Aravalli Orogenic Belt, there is a rhyodacite that yielded a zircon age of 1854 ± 7 Ma (Deb et al., 2002).

In the Singhbhum Craton, to the east of the Bastar Craton, the 'Newer Dolerites' intrude the Archean basement rocks and are thought to be Paleoproterozoic (≥ 1960 Ma) but the dykes have yielded a range of ages from ~2100 Ma to ~950 Ma including an age of ~1250 Ma (Saha and Mazumder, 2012; Sengupta and Ray, 2012; Shankar et al., 2014). Shankar et al. (2014) reported two baddeleyite Pb-Pb ages of dykes correlative with the 'Newer Dolerites (Pipilia swarm)' of 1766.2 ± 1.1 Ma and 1764.5 ± 0.9 Ma. There is another poorly constrained dyke swarm referred to as the Bhagamunda swarm which appears to be older than the New Dolerites (~1.77 Ga) but younger than the Ghatgaon (~2.26 Ga) dyke swarm (Samal et al., 2019). The uncertainty of the emplacement age and the compositional variability of the 'Newer Dolerites' suggest there could be one or more distinct swarms within the Singhbhum Craton but at this time, although still possible, they are unlikely to be related to the Sonakhan dykes or BCDS.

There is evidence to suggest there was widespread magmatism in the Indian Shield from ~1.88 Ga to ~1.85 Ga and possibly younger. However, due to the poor precision of the reported ages of basalts and other Paleoproterozoic mafic dykes in the Bundelkhand and Singhbhum Cratons any regional correlation at this time is uncertain. The age gap between the BCDS and SDS precludes a direct relationship between the two dyke swarms but it is still possible, due to their spatial association, that they may be related to the same regional rifting event. For example, the emplacement of the SDS may simply represent the migration of a mantle plume or, more likely, the propagation of a rift from the Dharwar Craton to the Bastar Craton (Sheppard et al., 2017). In any case, it appears the Sonakhan dyke swarm is distinct from other dyke swarms of the Indian Shield.

6.3. Prolonged break-up between India and Western Australia

Paleoproterozoic supercontinent reconfigurations suggest that Peninsular India and Western Australia were proximal from ~2100 Ma to ~1900 Ma and possibly as early as ~2350 Ma (Liu et al., 2018; Mohanty, 2012, 2015a). Specifically, paleomagnetic, geochemical, and geochronological studies of 1880 Ma dykes from the Yilgarn (Boonadgin), Bastar (Bastar-Cuddapah), and Dharwar (Bastar-Cuddapah) Cratons indicates that it is very likely the three were spatially associated before dyke emplacement and subsequently drifted apart (Liu et al., 2018; Shellnutt et al., 2018; Stark et al., 2018). The tectonic evolution of the Satpura Mountains of Central India temporally matches the evolution of the Capricorn Orogeny of Western Australia. Furthermore, the Glenburgh Terrane (within the Capricorn Orogeny) is considered to be exotic with respect to the Yilgarn or Pilbara Cratons but bears some lithological similarity to the cratonic rocks of the Bastar Craton (Mohanty, 2012; Mohanty, 2015b; Occhipinti et al., 2004; Saha and Mazumder, 2012; Sheppard et al., 2016).

The age of the SDS is broadly similar to a number of tectonomagmatic features of Peninsular India including the eruption age of felsic tuffs and mafic sills within the Cuddapah Basin (Belica et al., 2014; Sheppard et al., 2017). The known size of the SDS is comparatively small with respect to the Bastar-Cuddapah dyke swarm suggesting it may be representative of local rifting rather than regional. However, Ameen and Wilde (2006) reported an age of 1854 ± 5 Ma for a west trending mafic dyke in the northern Yilgarn Craton that cross-cuts the Yalgoo greenstone belt and is referred to as the Yalgoo dyke or Yalgoo dyke swarm. The Yalgoo dyke is compositionally similar to the high Mg#, high SiO_2 dykes described in this study (Figs. 6 and 7). The implication is that the Yalgoo dyke may be the first evidence for a regionally extensive dyke swarm that extended from the Bastar Craton to the Yilgarn Craton.

Liu et al. (2018) postulated a mantle plume model for the 1.88 Ga Bastar-Cuddapah-Boonadgin dykes and provided a plume centre location that may explain the dyke orientations and the proximity of India and Western Australia (c.f. French et al., 2008; Srivastava and Samal, 2018). The 30 million year age gap between the Bastar-Cuddapah-Boonadgin dykes and the Sonakhan-Cuddapah-Yalgoo dykes could be associated with renewed magmatic activity within a mantle plume regime or simply by rift propagation. The geochemical evidence in favour of a mantle plume origin of the SDS is limited although the correlation with the Yalgoo dyke does suggest a much larger event took place. Sheppard et al. (2017) argue against a mantle plume model to explain the volcanic cyclicity within the Cuddapah Basin precisely due to the prolonged and periodic nature of magmatism. The magmatic age gap is difficult to explain as it is relatively rare that peak magmatism associated with singular mantle plume spans more than ~10 million years, although there are exceptions (Bryan and Ernst, 2008). It is possible that the gap in magmatism was caused by the movement of thicker lithosphere over the plume head. In this scenario, the resumption of magmatism would occur as soon as lithosphere became thinner. However, the 'thick plate passage' model still does not address the geochemical evidence in favour of shallow mantle melting nor is it a likely reason for a complete cessation of magmatism over an area >900,000 km^2. Therefore, we think that the most likely explanation for the magmatic age is prolonged rift propagation.

There are many examples that show rifting, magmatism, and plate separation occur over a period of tens of millions of years. For example, the basalt of the Central Atlantic Magmatic Province erupted ~30 million years before plate separation (Biari et al., 2017). We suggest that the Sonakhan-Cuddapah-Yalgoo dykes were emplaced as rifting extended east to northeastward relative to the plume centre proposed by Liu et al. (2018). The migration of the rift coupled with tensional plate stress and regional structural weaknesses in the crust could explain the NNW trend of the Sonakhan dykes and the east-west trend of the Yalgoo dykes (Fig. 12). In other words, it is possible that the region was affected by triple-junction migration (Bird et al., 1999; Tesfaye et al., 2003). Ultimately the consequence of prolonged rifting was the break-up of India and Western Australia and the initiation of sea-floor spreading sometime shortly after 1850 Ma.

7. Conclusions

The NNW trending Sonakhan tholeiitic dykes of the northern Bastar Craton were emplaced at 1.85 Ga. There are two distinct groups of dykes based on Mg# and bulk TiO_2 contents. Rocks with high Mg# (>50) can be further subdivided into high (>52 wt%) and low (<52 wt%) SiO_2 groups. The high Mg#, low SiO_2 dykes are likely representative of the most 'primitive' and uncontaminated dykes within the SDS. The high Mg#, high SiO_2 dykes likely have the same origin as the high Mg#, low SiO_2 dykes but they were variably contaminated by crustal melts during emplacement or differentiation. The low Mg# (<50) dyke compositions can be explained by fractional crystallization of olivine, plagioclase and clinopyroxene of a parental magma similar to a high Mg# and low SiO_2 dyke. It is possible that some of the low Mg# dykes were also contaminated by crustal melts during emplacement. Trace element ratios ($Dy/Dy^* < 1.1$, $Tb/Yb_N < 1.8$), Sr-Nd isotopes ($^{87}Sr/^{86}Sr_{initial} = 0.7045$; $\varepsilon Nd(t) = 0 \pm 1$), and partial melting modeling indicate that the most primitive, uncontaminated dykes were derived from a subcontinental lithospheric mantle source that was lherzolitic and spinel-bearing. The limited geographic extent of the SDS and the likelihood that they were generated by partial melting from a shallow mantle source suggest that they were not likely derived from a mantle plume. However, they were emplaced shortly after the much larger and radially extensive Bastar-Cuddapah (1.88 Ga) dyke swarm (BCDS). It is possible that the SDS represents the youngest period of magmatism associated with the prolonged break-up of a supercontinent that comprised India and Western Australia. The apparent correlation between the SDS and the Yalgoo dykes of the Yilgarn Craton is additional supportive evidence that India and Western Australia were geological connected during the Orosirian Period of the Paleoproterozoic and subsequently drifted apart sometime after 1.85 Ga.

Acknowledgements

We thank Wen-Yu Hsu and Carol Chuang for their laboratory assistance. Comments by Rajesh Srivastava and an anonymous reviewer improved this manuscript. This research was supported by funding provided by MOST (Taiwan) grant #102-2628-M-003-001-MY4 to JGS.

Appendix A. Supplementary data

Supplementary data to this article can be found online at https://doi.org/10.1016/j.lithos.2019.03.015.

References

Ameen, S.M.M., Wilde, S.A., 2006. Identification of 1.85 Ga mafic dykes in the Northern Yilgarn Craton: A relationship to the Columbia Supercontinent? In: Zhang, J., He, Y., Yin, C., Leung, W. (Eds.), IAGR Annual Convention & International Symposium Abstracts & Program 2006, pp. 39–40

Belica, M.E., Piispa, E.J., Meert, J.G., Pesonen, L.J., Plado, J., Pandit, M.K., Kamenov, G.D., Celestino, M., 2014. Paleoproterozoic mafic dyke swarms from the Dharwar craton; paleomagnetic poles for India from 2.37 to 1.88 Ga and rethinking the Columbia supercontinent. Precambrian Research 244, 100–122.

Biari, Y., Klingelhoefer, F., Sahabi, M., Funck, T., Benabdellouahed, M., Schnabel, M., Reichert, C., Gutscher, M.-A., Bronner, A., Austin, J.A., 2017. Opening of the Central Atlantic Ocean: implications for geometric rifting and asymmetric initial seafloor spreading after continental breakup. Tectonics 36, 1129–1150.

Bird, R.T., Tebbens, S.F., Kleinrock, M.C., Naar, D.F., 1999. Episodic triple-junction migration by rift propagation an microplates. Geology 27, 911–914.

Bryan, S.E., Ernst, R.E., 2008. Revised definition of large igneous provinces (LIPs). Earth-Science Reviews 86, 175–2002.

Cagney, N., Crameri, F., Newsome, W.H., Lithgow-Bertelloni, C., Cotel, A., Hart, S.R., Whitehead, J.A., 2016. Constraining the source of mantle plumes. Earth and Planetary Science Letters 435, 55–63.

Clark, C., Fitzsimons, I.C.W., Healy, D., Harley, S.L., 2011. How does the continental crust get really hot? Elements 7, 235–240.

Crawford, A.R., Compston, W., 1970. The age of the Vindhyan system of Peninsular India. Quarterly Journal of the Geological Society 125, 351–371.

Das, N., Royburman, K.J., Vatsa, U.S., Mahurkar, Y.V., Dhoundial, D.P., 1990. Sonakhan Schist Belt, a Precambrian granite–greenstone complex. Geological Survey of India 28, 118–132 Special Publication.

Das, K., Yokoyama, K., Chakraborty, P.P., Sarkar, A., 2009. Basal tuffs and contemporaneity of the Chattisgarh and Khariar basins based on new dates and geochemistry. Journal of Geology 117, 88–102.

Das, P., Das, K., Chakraborty, P.P., Balakrishnan, S., 2011. 1420 Ma diabase intrusives from the Mesoproterozoic Singhora Group, Chhattisgarh Supergroup, India: implications towards non-plume intrusive activity. Journal of Earth System Science 120, 223–236.

Davidson, J., Turner, S., Plank, T., 2013. Dy/Dy*: variation arising from mantle sources and petrogenetic processes. Journal of Petrology 54, 525–537.

Deb, M., Thorpe, R., Krstic, D., 2002. Hindoli Group rocks in the eastern fringe of the Aravalli-Delhi orogenic belt-Archean secondary greenstone belt or Proterozoic supracrustals? Gondwana Research 5, 879–883.

Deshmukh, S.D., Hari, K.R., Diwan, P., Manu Prasanth, M.P., 2017. Geochemistry and petrogenesis of felsic meta-volcanic rocks of Baghmara Formation, Sonakhan Greenstone Belt, Central India. Journal of Geosciences Research 2, 69–74.

Dhang, P.C., Patranabis-Deb, S., 2011. Lithostratigraphy of the Chhattisgarh Supergroup around Singhora-Saraipali area and its tectonic implications. Memoir of the Geological Society of India 77, 493–515.

Ernst, R.E., 2014. Large Igneous Provinces. Cambridge University Press, Cambridge, UK, p. 653.

Ernst, R.E., Bleeker, W., 2010. Large igneous provinces (LIPs), giant dyke swarms, and mantle plumes: significance for breakup events within Canada and adjacent regions from 2.5 Ga to the present. Canadian Journal of Earth Sciences 47, 695–739.

French, J.E., Heaman, L.M., 2010. Precise U-Pb dating of Paleoproterozoic mafic dyke swarms of the Dharwar craton, India: implications for the existence of the Neoarchean supercraton Sclavia. Precambrian Research 183, 416–441.

French, J.E., Heaman, L.M., Chacko, T., Srivastava, R.K., 2008. 1891-1883 Ma Southern Bastar-Cuddapah mafic igneous events, India: a newly recognized large igneous province. Precambrian Research 160, 308–322.

Ghosh, S., Rajajaiya, V., Ashiya, I.D., 1995. Rb-Sr dating of components from the Sonakhan granite-greenstone belt, Raipur district. M. P. Records Geological Survey of India 128, 11–13.

Goldberg, A.S., 2010. Dyke swarms as indicators of major extensional events in the 1.9-1.2 Ga Columbia supercontinent. Journal of Geodynamics 50, 176–190.

Halls, H.C., 1982. The importance and potential of mafic dyke swarms in studies of geodynamic processes. Geoscience Canada 9, 145–154.

Herzberg, C., Asimow, P.D., Arndt, N., Niu, Y., Lesher, C.M., Fitton, J.G., Cheadle, M.J., Saunders, A.D., 2007. Temperatures in ambient mantle and plumes; constraints from basalts, picrites, and komatiites. Geochemistry, Geophysics, Geosystems 8. https://doi.org/10.1029/2006GC001390 Q02006.

Krishnamurthy, P., Sinha, D.K., Singh, S.N., 1988. Geology, geochemistry and genesis of metabasalts, metarhyolites and associated U mineralization at Bodal, Rajnandgaon district, M.P., and implications for U mineralization in Central India. Exploration and Research for Atomic Minerals 1, 13–19.

Kumar, A., Hamilton, M.A., Halls, H.C., 2012. A Paleoproterozoic giant radiating dyke swarm in the Dharwar Craton, southern India. Geochemistry, Geophysics, Geosystems 13, Q02011. https://doi.org/10.1029/2011GC003926.

LeBas, M.J., LeMaitre, R.W., Streckeisen, A., Zanettin, B., 1986. A chemical classification of volcanic rocks based on the total alkali-silica diagram. Journal of Petrology 27, 745–750.

Liao, A.C.-Y., Shellnutt, J.G., Hari, K.R., Denyszyn, S.W., Vishwakarma, N., Verma, C.B., 2019. A petrogenetic relationship between 2.37 Ga boninitic dyke swarms of the Indian Shield: evidence from the Central Bastar Craton and NE Dharwar Craton. Gondwana Research https://doi.org/10.1016/jgr.2018.12.007.

Liu, Y., Li, Z.-X., Pisarevsky, S.A., Kirscher, U., Mitchell, R.N., Stark, J.C., 2018. Palaeomagnetism of the 1.89 Ga Boonadgin dykes of the Yilgarn Craton: possible connection with India. Precambrian Research https://doi.org/10.1016/j.precamres.2018.05.021.

Ludwig, K.R., 2011. Isoplot v. 4.15: A Geochronological Toolkit for Microsoft Excel. vol. 4. Berkeley Geochronology Center Special Publication, p. 70.

Manikyamba, C., Santosh, M., Chandan Kumar, B., Rambabu, S., Li, T., Saha, A., Khelen, A.C., Ganguly, S., Singh, T.D., Subba Rao, D.V., 2016. Zircon U-Pb geochronology, Lu-Hf isotope systematics, and geochemistry of bimodal volcanic rocks and associated granitoids from Kotri Belt, Central India: implications for Neoarchean-Paleoproterozoic crustal growth. Gondwana Research 38, 313–333.

Meert, J.G., Pandit, M.K., Pradhan, V.R., Banks, J., Sirianni, R., Stroud, M., Newstead, B., Gifford, J., 2010. Precambrian crustal evolution of Peninsular India: a 3.0 billion year odyssey. Journal of Asian Earth Sciences 39, 483–515.

Mishra, D.C., Kumar, M.R., 2014. Proterozoic orogenic belts and rifting of Indian cratons: geophysical constraints. Geoscience Frontiers 5, 25–41.

Mohanty, S., 2012. Spatio-temporal evolution of the Satpura Mountain Belt of India: a comparison with the Capricorn Orogen of Western Australia and implication for evolution of the supercontinent Columbia. Geoscience Frontiers 3, 241–267.

Mohanty, S., 2015a. Precambrian continent assembly and dispersal events of South Indian and East Antarctic Shields. International Geology Review 57, 1992–2027.

Mohanty, S., 2015b. Palaeoproterozoic supracrustals of the Bastar Craton: Dongargarh Supergroup and Sausar Group. In: Mazumder, R., Eriksson, P.G. (Eds.), Precambrian Basins of India: Stratigraphic and Tectonic Context. vol. 43. Geological Society, London, Memoirs, pp. 151–164.

Mondal, M., Raza, M., 2009. Tectonomagmatic evolution of the Bastar craton of Indian shield through plume-arc interaction: evidence from geochemistry of the mafic and felsic volcanic rocks of Sonakhan greenstone belt. Journal of the Virtual Explorer 32, 3.

Mondal, S.K., Ripley, E.M., Li, C., Frei, R., 2006. The genesis of Archaean chromites from the Muasahi and Sukinda massifs in the Singhbhum craton, India. Precambrian Research 148, 45–66.

Murthy, M.G.L., 1995. Proterozoic mafic dykes in southern Peninsular India: a review. In: Devaraju, T.C. (Ed.), Dyke Swarms of Peninsular India. vol. 33. Geological Society of India Memoir, pp. 81–98.

Naqvi, S.M., Rogers, J.J.W., 1987. Precambrian Geology of India. Oxford University Press, New York, p. 223.

Nicholls, J., Russell, J.K., 2016. Pearce element rations diagrams: linking geochemical data to magmatic processes. Geoscience Canada 43, 133–146.

Occhipinti, S.A., Sheppard, S., Passhier, C., Tyler, I.M., Nelson, D.R., 2004. Palaeoproterozoic crustal accretion and collision in the southern Capricorn Orogen: the Glenburgh Orogeny. Precambrian Research 128, 237–255.

Pascoe, E.H., 1973. A Manual of the Geology of India and Burma. 3rd ed. pp. 1472–2017.

Patranabis-Deb, S., Bickford, M.E., Hill, B., Chaudhuri, A.K., Basu, A., 2007. SHRIMP ages of zircon in the uppermost tuff in Chattisgarh Basin in Central India required ~500 Ma adjustment in Indian Proterozoic stratigraphy. Journal of Geology 115, 407–415.

Pearce, J.A., 2008. Geochemical fingerprinting of oceanic basalts with applications to ophiolite classification and the search for Archean oceanic crust. Lithos 100, 14–48.

Pearce, J.A., Norry, M.J., 1979. Petrogenetic implications of Ti, Zr, Y and Nb variations in volcanic rocks. Contributions to Mineralogy and Petrology 69, 33–47.

Pradhan, V.R., Meert, J.G., Pandit, M.K., Kamenov, G., Modal, M.E.A., 2012. Paleomagnetic and geochronological studies of the mafic dyke swarms of Bundelkhand craton, Central India: implications for the tectonic evolution and paleogeographic reconstructions. Precambrian Research 198-199, 51–76.

Manu Prasanth, M.P., Hari, K.R., Chalapathi Rao, N.V., Hou, G., Pandit, D., 2018. An island-arc tectonic setting for the Neoarchean Sonakhan greenstone belt, Bastar Craton, Central India: insights from the chromite mineral chemistry and geochemistry of the siliceous high-Mg basalts (SHMB). Geological Journal 53, 1526–1542.

Radhakrishna, B.P., Naqvi, S.M., 1986. Precambrian continental crust of India and its evolution. Journal of Geology 94, 145–166.

Radhakrishna, T., Maluski, H., Mitchell, J.G., Joseph, M., 1999. $^{40}Ar/^{39}Ar$ and K/Ar geochronology of the dykes from the south Indian granulite terrain. Tectonophysics 304, 109–129.

Rajesh, H.M., Mukhopadhyay, J., Beukes, N.J., Gutzmer, J., Belyanin, G.A., Armstrong, R.A., 2009. Evidence for an early Archaean granite from Bastar craton, India. Journal of the Geological Society, London 166, 193.

Ramakrishnan, M., Vaidyanadhan, R., 2010. Geology of India. vol. 1. Geological Society of India, p. 556.

Rao, J.M., Rao, G.V.S.P., Widdowson, M., Kelley, S.P., 2005. Evolution of Proterozoic mafic dyke swarms of the Bundelkhand granite massif, Central India. Current Science 88, 502–506.

Rogers, J.J.W., Santosh, M., 2004. Continents and Supercontinents. Oxford University Press, New York, p. 289.

Rudnick, R.L., Gao, S., 2003. Composition of the continental crust. In: Rudnick, R.L. (Ed.), The Crust. Treatise of Geochemistry vol. 3, pp. 1–64.

Saha, D., Mazumder, R., 2012. An overview of the Palaeoproterozoic geology of Peninsular India, and key stratigraphic tectonic issues. In: Mazumder, R., Saha, D. (Eds.), Palaeoproterozoic of India. vol. 365. Geological Society, London, Special Publications, pp. 5–29.

Samal, A.K., Srivastava, R.K., Ernst, R.E., Söderlund, U., 2019. Neoarchean-Mesoproterozoic mafic dyke swarms of the Indian Shield mapped using Google Earth™ images and ArcGIS™, and links with large igneous provinces. In: Srivastava, R.K., Ernst, R.E., Peng, P. (Eds.), Dyke Swarms of the World: A Modern Perspective. Springer Geology, pp. 335–390.

Santosh, M., 2012. India's Palaeoproterozoic legacy. In: Mazumder, R., Saha, D. (Eds.), Palaeoproterozoic of India. vol. 365. Geological Society, London, Special Publications, pp. 263–288.

Sarkar, G., Corfu, F., Paul, D.K., McNaughton, N.J., Gupta, S.N., Bishui, P.K., 1993. Early Archean crust in Bastar Craton, Central India – a geochemical and isotopic study. Precambrian Research 62, 127–137.

Sarkar, A., Bodas, M.S., Kundu, H.K., Mamgain, V.V., Shankar, R., 1998. Geochronology and geochemistry of Mesoproterozoic intrusive plutonites from the eastern segment of the Mahakoshal greenstone belt, Central India. IGCP-368 Seminar on Precambrian Crust in Eastern and Central India, Bhubaneshwar, pp. 82–85.

Sawyer, E.W., Cesare, B., Brown, M., 2011. When the continental crust melts. Elements 7, 229–234.

Sengupta, P., Ray, A., 2012. Newer Dolerite dykes, Jharkhand, India: a case study of magma generation, differentiation and metasomatism in a subduction zone setting. Geochemical Journal 46, 477–491.

Shankar, R., Vijayagopal, B., Kumar, A., 2014. Precise Pb-Pb baddeleyite ages of 1765 Ma for a Singhbhum 'newer dolerite' dyke swarm. Current Science 106, 1306–1310.

Sharma, R.S., 2009. Cratons and Fold Belts of India. Springer, Berlin, p. 304.

Shellnutt, J.G., MacRae, N.D., 2012. Petrogenesis of the Mesoproterozoic (1.23 Ga) Sudbury dyke swarm and its questionable relationship to plate separation. International Journal of Earth Sciences 101, 3–23.

Shellnutt, J.G., Hari, K.R., Liao, A.C.-Y., Denyszyn, S.W., Vishwakarma, N., 2018. A 1.88 Ga giant radiating mafic dyke swarm across Southern India and Western Australia. Precambrian Research 308, 58–74.

Sheppard, S., Fletcher, I.R., Rasmussen, B., Zi, J.-W., Muhling, J.R., Occhipinti, S.A., Wingate, M.T.D., Johnson, S.P., 2016. A new Paleoproterozoic tectonic history of the eastern Capricorn Orogen, Western Australia, revealed by U-Pb zircon dating of micro-tuffs. Precambrian Research 286, 1–19.

Sheppard, S., Rasmussen, B., Zi, J.-W., Somasekhar, V., Sarma, D.S., Ram Mohan, M., Krapež, B., Wilde, S.A., McNaughton, N.J., 2017. Sedimentation and magmatism in the Paleoproterozoic Cuddapah Basin, India: consequences of lithospheric extension. Gondwana Research 48, 153–163.

Smith, P.M., Asimow, P.D., 2005. Adiabat_1ph: a new public front-end to the MELTS, pMELTS, and pHMELTS models. Geochemistry, Geophysics, Geosystems 6, Q02004. https://doi.org/10.1029/2004GC000816.

Söderlund, U., Johansson, L., 2002. A simple way to extract baddeleyite (ZrO_2). Geochemistry, Geophysics, Geosystems 3, 1014. https://doi.org/10.1029/2001GC000212.

Söderlund, U., Bleeker, W., Demirer, K., Srivastava, R.K., Hamilton, M., Nilsson, M., Pesonen, L.J., Samal, A.K., Jayananda, M., Ernst, R.E., Srinivas, M., 2018. Emplacement ages of Paleoproterozoic mafic dyke swarms in eastern Dharwar craton, India: implications for paleoreconstructions and support for a ~30o change in dyke trends from south to north. Precambrian Research https://doi.org/10.1016/j.precamres.2018.12.017.

Srivastava, R.K., Gautam, G.C., 2015. Geochemistry and petrogenesis of Paleo-Mesoproterozoic mafic dyke swarms from northern Bastar craton, Central India: geodynamic implications in reference to Columbia supercontinent. Gondwana Research 28, 1061–1078.

Srivastava, R.K., Samal, A.K., 2018. Geochemical characterization, petrogenesis, and emplacement tectonics of Paleoproterozoic high-Ti and low-Ti mafic intrusive rocks from the western Arunachal Himalaya, northeastern India and their possible relation to the ~1.9 Ga LIP event of the Indian shield. Geological Journal 54, 245–265.

Srivastava, R.K., Söderlund, U., Ernst, R.E., Mondal, S.K., Samal, A.K., 2018. Precambrian mafic dyke swarms in the Singhbhum craton (eastern India) and their links with dyke swarms of the eastern Dharwar craton (southern India). Precambrian Research https://doi.org/10.1016/j.precamres.2018.08.001.

Stark, J.C., Wang, X.-C., Denyszyn, S.W., Li, Z.-X., Rasmussen, B., Zi, J.-W., Sheppard, S., 2018. Newly identified 1.89 Ga mafic dyke swarm in the Archean Yilgarn Craton, Western Australia suggests a connection with India. Precambrian Research https://doi.org/10.1016/j.precamres.2017.12.036.

Sun, S.-S., McDonough, W.F., 1989. Chemical and isotopic systematics of oceanic basalts: implications for mantle composition and process. In: Saunders, A.D., Norry, M.J. (Eds.), Magmatism in the Ocean Basins. vol. 42. Geological Society, London, Special Publications, pp. 313–345.

Tesfaye, S., Harding, D.J., Kusky, T.M., 2003. Early continental breakup boundary and migration of the Afar triple junction, Ethiopia. Geological Society of America Bulletin 115, 1053–1067.

Wang, K., Plank, T., Walker, J.D., Smith, E.I., 2002. A mantle melting profile across the Basin and Range, SW USA. Journal of Geophysical Research 107. https://doi.org/10.1029/2001JB0002009.

Workman, R.K., Hart, S.R., 2005. Major and trace element composition of the depleted MORB mantle (DMM). Earth and Planetary Science Letters 231, 53–72.

Yale, L.B., Carpenter, S.J., 1998. Large igneous provinces and giant dike swarms: proxies for supercontinent cyclicity and mantle convection. Earth and Planetary Science Letters 163, 109–122.

Zhao, G., Cawood, P.A., Wilde, S.A., Sun, M., 2002. Review of global 2.1–1.8 Ga orogens: implications for a pre-Rodinia supercontinent. Earth-Science Reviews 59, 125–162.